International Journal of Pharmaceutics: X 1 (2019) 100008

Contents lists available at ScienceDirect

International Journal of Pharmaceutics: X

journal homepage: www.journals.elsevier.com/international-journal-of-pharmaceutics-x

The role interplay between mesoporous silica pore volume and surface area and their effect on drug loading capacity

Christoffer G. Bavnhøj[a], Matthias M. Knopp[b,*], Cecilie M. Madsen[c], Korbinian Löbmann[a]

[a] Department of Pharmacy, University of Copenhagen, DK-2100 Copenhagen, Denmark
[b] Bioneer: FARMA, Department of Pharmacy, DK-2100 Copenhagen, Denmark
[c] Pharmaceutical R&D, H. Lundbeck A/S, DK-2500 Valby, Denmark

ARTICLE INFO

Keywords:
Mesoporous silica
Loading capacity
Differential scanning calorimetry (DSC)
Poorly soluble drugs
Amorphous stability
Surface area
Pore volume
Pore diameter

ABSTRACT

In this study, the influence of the mesoporous silica (MS) textural properties (surface area, pore diameter, and pore volume) on drug loading capacity (monomolecular loading capacity and pore filling capacity) was investigated theoretically and experimentally using a thermoanalytical method. The loading capacities of three model drugs (celecoxib, cinnarizine, and paracetamol) were determined in five different MS grades of Sylysia® with identical chemical composition, but varying surface area, pore diameter and pore volume. The experimentally determined loading capacities were compared to theoretical loading capacities, calculated based on the surface area and amorphous density of the drugs, and the surface area and pore volume of the MS. The findings of the study showed that the monomolecular loading capacity generally increased with increasing surface area and decreasing pore volume of the MS. However, the MS grade with the highest surface area did not display the highest monomolecular loading capacity for any of the three drugs. This was probably a result of the decreasing pore diameter necessary to accommodate the increasing surface area of the MS i.e., if the pore is smaller than the drug molecule, the drug cannot access the available surface area. For these systems, the amorphous density of the drug and the pore volume of the MS was used to estimate the theoretical pore filling capacity, which was in good agreement with the experimentally determined loading capacity. In conclusion, this study showed that both the pore volume and surface area of the MS will have an influence on the drug loading capacity and that this can be estimated with good accuracy both theoretically and experimentally.

1. Introduction

The use of mesoporous silicas (MS) in amorphous drug delivery systems is gaining increasing interest in the pharmaceutical field due to their ability to stabilize the amorphous form of a drug (Rouquerol et al., 1994; Rengarajan et al., 2008; Shen et al., 2010; Laitinen et al., 2013; Jackson et al., 2014; Kumar et al., 2014). Several studies have also shown that drug-loaded MS systems not only have an increased *in vitro* dissolution rate and apparent solubility compared to the crystalline drug alone, but the *in vivo* performance may also be improved (Heikkilä et al., 2007; Mellaerts et al., 2008; Qian and Bogner, 2011; Hillerström et al., 2014; McCarthy et al., 2016).

Due to their small pores (2–50 nm), MS have large specific surface areas (often greater than 300 m^2/g), which offer significant additional surface free energy. Therefore, adsorption of drugs on the surface of an MS may allow the system to progress to a lower free energy state, thus, stabilizing the amorphous drug (Azaïs et al., 2006; Qian and Bogner, 2011). Furthermore, if the pore diameter is smaller than the critical crystal nuclei, the MS may also prevent crystallization of the amorphous form through spatial confinement (Andersson et al., 2004; Rengarajan et al., 2008; Qian and Bogner, 2012; Yani et al., 2016). Hence, two mechanisms have been proposed for amorphous stabilization: I) non-covalent interactions (e.g. hydrogen bonding) between the drug molecules, and the MS surface II) spatial separation/confinement of the drug in MS pores. For these mechanisms, the loading capacity can be defined as I) a drug monomolecular layer covering the surface of the MS, i.e. monomolecular loading capacity (MLC), and II) filling the pores of the MS, i.e. pore filling capacity (PFC). From these two definitions, it is clear that the surface area and pore volume of the MS will have a significant influence on the drug loading capacities. The influence of these two MS properties on the drug loading capacity has been reported previously, but the results are inconclusive. For example, Qu et al. (2006) showed that the loading capacity of captopril increased with increasing MS surface area, while Zhang et al. (2010) showed that the

* Corresponding author at: Bioneer: FARMA, Department of Pharmacy, Universitetsparken 2, DK-2100 Copenhagen, Denmark.
E-mail address: mmk@bioneer.dk (M.M. Knopp).

https://doi.org/10.1016/j.ijpx.2019.100008
Received 6 December 2018; Received in revised form 7 February 2019; Accepted 9 February 2019
Available online 22 February 2019

loading capacity of telmisartan increased with increasing MS pore volume. Another major drawback is that the drug loading capacity is inconsistently reported even for the same drug-MS system (Charnay et al., 2004; Limnell et al., 2011; Lai et al., 2017). The reason for this could be the use of different loading techniques (Qian and Bogner, 2012; Ahern et al., 2013). For example, Ahern et al. (2013) showed that the loading capacity of fenofibrate in SBA-15 was higher when using melt-fusion compared to the solvent impregnation and Limnell et al. (2011) showed that the loading capacity of indomethacin in Syloid 244 FP was significantly lower when using solvent immersion compared to rotary evaporation and fluid bed. Finally, Hong et al. (2016) demonstrated that solvent impregnation caused fenofibrate to accumulate outside the pores of the MS, which resulted in crystallization.

To overcome the aforementioned inconsistencies regarding the drug loading capacity determinations, Hempel et al. (2018) recently introduced a differential scanning calorimetry (DSC)-based method to determine the MLC for drugs with good glass-forming ability. Using the proposed method, it is possible to determine the true maximum MLC independent of loading technique. Furthermore, the study showed that drug loading below the experimentally determined MLC resulted in thermodynamically stable amorphous systems.

Thus, using this method, the present study aimed to systematically determine the influence of surface area, pore size, and pore volume of the MS on the drug loading capacities (MLC and PFC). For this purpose, the MLC and PFC of three model drugs celecoxib (CCX), cinnarizine (CIN), and paracetamol (PAR) in five different MS (Sylysia®) grades were determined. All the model drugs were good glass-formers and the Sylysia® grades all had identical chemical composition, but varying surface area, pore size, and pore volume. Thus, any non-covalent interactions between the drug molecules and the MS surface will be identical between grades, which is a prerequisite to enable this comparative study. The experimental monomolecular loading capacities (xMLC) were compared to the theoretical loading capacities (tMLC and tPFC), calculated based on the surface area and amorphous density of the drugs and surface area and pore volume of the MS.

2. Experimental section

2.1. Materials

Celecoxib (CCX, M_w = 381.4 g/mol) was purchased from Dr. Reddy's (Hyderabad, India), cinnarizine (CIN, M_w = 368.5 g/mol) was purchased from Sigma-Aldrich Co. (St. Louis, MO, USA) and paracetamol (PAR, M_w = 151.2 g/mol) was purchased from Fagron (Rotterdam, The Netherlands). The different MS grades (Sylysia® SY240, SY350, SY430, SY550, and SY730) were kindly gifted by Fuji Silysia Chemical Ltd (Kasugai Aichi, Japan). The textural properties of SY240, SY350, SY430, SY550, and SY730 are listed in Table 1 and the physico-chemical properties of the CCX, CIN, and PAR are summarized in Table 2.

2.2. Nitrogen adsorption

The surface areas of the different MS grades were determined by nitrogen adsorption at −196 °C using a TriStar 3020 from Micrometrics Instrument Corp. (Norcross, GE, USA). Sample sizes were in the range of 24–70 g and all samples were degassed at 60 °C for 24 h prior to analysis under 1.5 bar nitrogen gas purge. The Brunauer-Emmet-Teller (BET) specific surface areas were extracted from single measurements using the TriStar II software (version 3.02) at relative pressure P/P_0 = 0.30 and were similar to the surface areas provided by the supplier.

Table 1
Specification of the different mesoporous silica (MS). The surface area was determined using nitrogen adsorption and average pore volume and diameter were provided by Fuji Silysia Chemical Ltd (Kasugai Aichi, Japan).

MS grade	SY240	SY350	SY430	SY550	SY730
Surface area (m^2/g)	272	268	559	634	682
Pore diameter (nm)	24	21	17	7.0	2.5
Pore volume (cm^3/g)	1.80	1.60	1.25	0.80	0.44

Table 2
Physico-chemical properties of the model compounds celecoxib (CCX), cinnarizine (CIN), and paracetamol (PAR). Glass transition temperature (T_g), change in heat capacity ($\triangle C_p$), melting temperature (T_m), and amorphous density were determined using DSC and minimal projection area was determined using MarvinSketch 18.10 from Chemaxon (Budapest, Hungary).

Model compound	CCX	CIN	PAR
T_g (°C)	59.2	8.0	24.3
$\triangle C_p$ (J/g·°C)	0.481	0.612	0.692
T_m (°C)	164.0	119.4	157.0
Amorphous density (g/cm^3)	1.35	1.22	1.06
M_w (g/mol)	381.4	368.5	151.2
Min. projection area (nm^2)	0.57	0.63	0.21

2.3. Helium pycnometry

The amorphous densities of the model drugs were determined using an AccuPyc 1330 helium pycnometer from Micromeritics Instruments Corp (Norcross, GA, USA). The amorphous drugs were prepared by melting samples of ~2 g in an electrical oven at 5 °C above their melting point (T_m) for 5 min and subsequent quench cooling by removing the samples from the oven. Prior to the density measurements, the samples were gently ground and accurately weighed into an aluminum sample holder and their amorphicity confirmed using X-ray powder diffraction (data not shown). The samples were purged with 19.5 psig dry helium in the pycnometer to determine the amorphous densities. The reported results were averages of 10 consecutive measurements.

2.4. Monomolecular loading capacity determinations

The experimental monomolecular loading capacity (xMLC) was determined using the heat-cool-heat method proposed by Hempel et al. (2018) Approximately 200 mg of physical mixtures of drug and MS with a drug fraction ranging from 50 to 100 wt% were prepared by gentle mixing using mortar and pestle. Samples of 2–4 mg were then analyzed in a DSC Q2000 from TA Instruments Inc. (New Castle, DE, USA). Initially, the samples were annealed at ~10 °C above the T_m of the respective drug for 5 min, followed by a rapid cooling to ~40 °C below the glass transition temperature (T_g) of the drug. After quenching, the samples were heated at a rate of 20 °C/min to determine the heat capacity (ΔC_p) over the T_g. The samples were run in duplicate and analyzed using the TRIOS software (version 4.3.0.38). A linear fitting of the determined $\triangle C_p$ as a function of drug fraction (wt%) was performed in order to determine the xMLC as X-intercept (zero $\triangle C_p$). A 95% prediction interval was determined as the upper- and lower limits of the X-intercept considering each replicate of $\triangle C_p$ as an individual data point (Hempel et al., 2018).

The reported T_m of the drugs were determined as onset temperature via the TRIOS software for the pure model drug (100 wt%). Thermogravimetric analysis (Discovery TGA, TA Instruments Inc., New Castle, DE, USA) showed that there was no thermal degradation under the thermal conditions applied during the DSC measurements.

3. Results and discussion

An example of the $\triangle C_p$ extrapolation for CCX-SY350 is shown in Fig. 1. For this system, the xMLC (X-intercept of the extrapolated

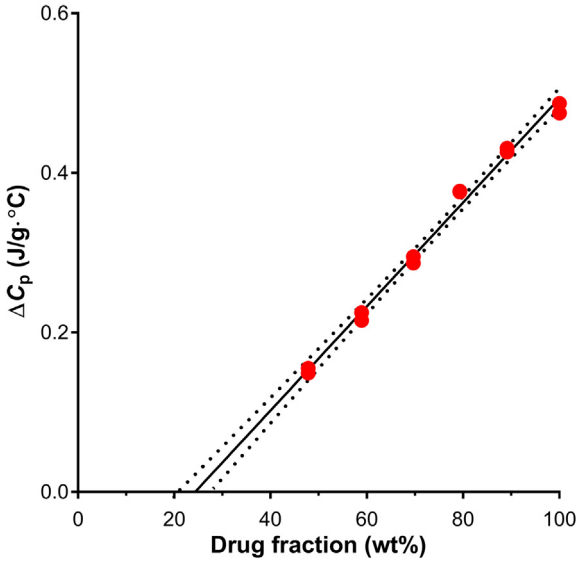

Fig. 1. Heat capacity ($\triangle C_p$) plotted as a function of drug fraction for CCX-SY350 after the heat-cool-heat cycle in the DSC. The data is extrapolated to zero $\triangle C_p$ through linear extrapolation (solid line, $r^2 = 0.995$) including the 95% confidence interval (dashed lines).

function) was found to be 24.3 wt%. The determined xMLC including the 95% prediction interval for the three model drugs in the five different MS grades are summarized in Table 3. All systems demonstrated a good linear relationship between drug fraction and $\triangle C_p$ with correlation coefficients (r^2) from 0.972 to 0.995.

Comparing the xMLC values for CCX in the different MS grades, it is evident that the xMLC for CCX-SY240 was similar to that obtained for CCX-SY350 (23.4 and 24.3 wt%, respectively). Given that SY240 and SY350 provide a similar surface area available for adsorption (271 and 267 m^2/g, respectively) this observation was somewhat expected. Furthermore, the increase in surface area between SY350 and SY430 (267 and 559 m^2/g, respectively) also resulted in an increase in the xMLC from 24.3 to 34.0 wt%. However, the increase in surface area between SY550 and SY730 (which had the largest surface area of 681 m^2/g), did not result in an increase in the xMLC.

The CIN systems generally displayed the same trend as observed for CCX with similar xMLC for CIN-SY240 and CIN-SY350 (21.2 and 24.3 wt%, respectively). The deviation of the xMLC values can be explained by the relatively large prediction interval for both systems; hence, the difference between the two means is not statistically significant. For CIN-SY350 and CIN-SY430, the larger MS surface area also resulted in an increase in xMLC from 24.3 to 33.8 wt%, respectively. However, interestingly, the xMLC for CIN-SY730 did not increase compared to CIN-SY550, but in fact decreased from 37.0 to 32.9 wt% despite the larger available surface area of SY730.

The PAR systems also displayed the same overall trend as CCX and CIN with a general increase in xMLC with increasing MS surface area from 24.4 to 39.6 wt% for PAR-SY240 and PAR-SY550, respectively. In accordance with the observations for CIN, a significant decrease in xMLC for PAR-SY730 compared to PAR-SY550 was observed (39.6 and 28.8 wt%, respectively). Furthermore, the xMLC obtained for PAR in all MS grades (except SY730) were higher than those obtained for CCX and CIN, which yielded similar xMLC. This can be explained by comparing the molecular size and thus, surface area of the three model drugs (see Table 2). As the molecular surface area of PAR is smaller compared to CCX and CIN, it also occupies a smaller area on the MS surface and therefore, the xMLC obtained for the PAR systems should also be higher in theory. Consequently, these findings strongly indicate that the thermoanalytical method proposed by Hempel et al. (2018) indeed is able to determine the MLC of drugs with good glass-forming ability in MS.

Table 4
Theoretical monomolecular loading capacity (tMLC) of CCX, CIN, and PAR in the different MS grades. The tMLC are calculated based on Eq. (1) and transformed to wt%.

		SY240	SY350	SY430	SY550	SY730
tMLC (wt%)	CCX	23.3	23.0	38.4	41.5	43.2
	CIN	21.0	20.8	35.4	38.3	40.0
	PAR	24.6	24.4	40.2	43.3	45.1

To elucidate the mechanism responsible for the deviation of the xMLC for the SY730 systems, a theoretical estimation of the MLCs was determined (tMLC). By assuming that drug molecules are able to cover the entire MS surface, the tMLC of any given system can be calculated from:

$$\text{tMLC} = \frac{A_{MS} \cdot M_{w(drug)}}{A_{drug} \cdot N_A} \quad (1)$$

where A_{MS} is the surface area of the respective MS (m^2/g), A_{drug} is the minimal projection area of the respective drug (m^2/molecule), N_A is the Avogadro constant ($6.022 \cdot 10^{23}\ mol^{-1}$), and $M_{w\ (drug)}$ is the molecular weight (g/mol) of the respective drug. Using Eq. (1), the tMLC is given as w_{drug}/w_{MS} so to enable a comparison with the xMLC, the tMLC was transformed to wt% i.e. $w_{drug}/(w_{drug} + w_{MS})$. Accordingly, the tMLC for all drug-MS systems are listed in Table 4 and plotted in Fig. 2 as a function of surface area along with the xMLC (Table 3).

As can be seen in Fig. 2, the tMLC for the three drugs in SY240, SY350, SY430, and SY550 are in good agreement with the xMLC. However, for CCX-SY730, CIN-SY730, and PAR-SY730 the tMLC is 7.4, 7.1, and 16.3 wt% higher than the xMLC, respectively, which is significantly above the 95% confidence intervals of the xMLC (see Tables 3 and 4). These findings suggest that a part of the available surface area of SY730 is not accessible for the drug molecules and, hence, results in lower than expected xMLC. This inconsistency could be due to the relatively small average pore size of SY730 of 2.5 nm, which may result in a spatial limitation. For example, some pores may be too narrow to accommodate the molecules to be adsorbed adjacently and other pores may simply be smaller than the drug molecule itself (cf. ~1 nm). Given that the tMLC (Eq. (1)) is obtained under the assumption that drug molecules are able to cover the entire MS surface, the spatial limitation is a very plausible explanation to the discrepancy observed between the tMLC and xMLC. Similar findings have been reported in literature, where the drug loading decreased with decreasing pore size despite an increase in surface area (Andersson et al., 2004; Charnay et al., 2004; Horcajada et al., 2004).

Based on these observations, it is evident that the larger surface area

Table 3
Experimentally determined monomolecular loading capacities (xMLC) for CCX, CIN, and PAR in the different MS grades. The 95% prediction interval is given in brackets.

		SY240	SY350	SY430	SY550	SY730
xMLC (wt%)	CCX	23.4 (20.0–26.4)	24.3 (20.7–27.5)	34.0 (30.3–37.3)	36.9 (32.7–40.4)	35.8 (31.8–39.3)
	CIN	21.2 (15.6–25.9)	24.3 (20.5–27.7)	33.8 (30.8–36.6)	37.0 (33.8–39.7)	32.9 (28.3–36.7)
	PAR	24.4 (17.2–30.2)	30.2 (27.4–32.8)	37.3 (31.6–41.8)	39.6 (34.8–43.5)	28.8 (23.4–33.3)

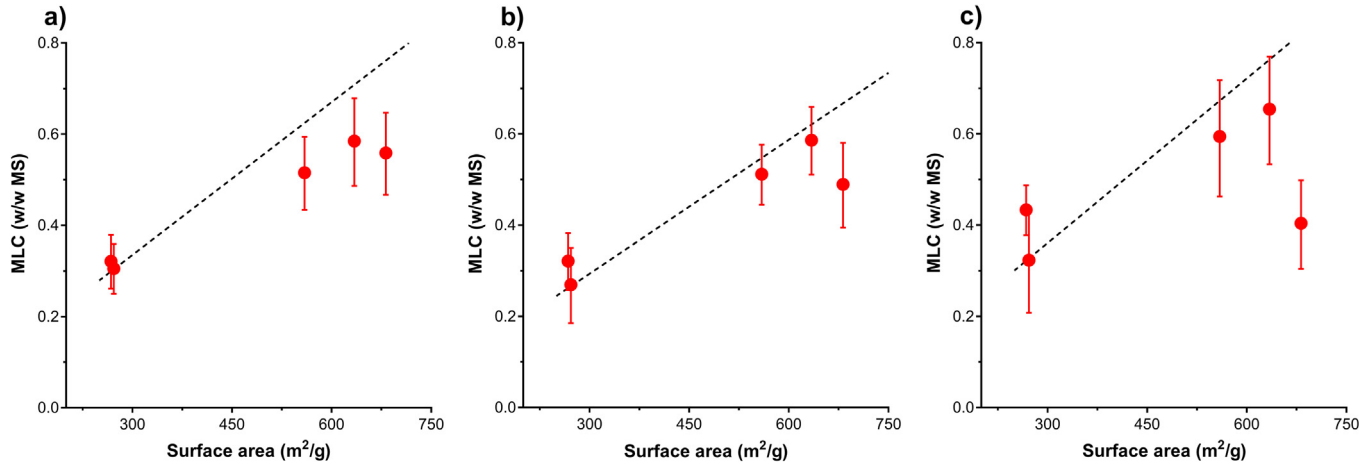

Fig. 2. MLC (in w_{drug}/w_{MS}) plotted as a function of MS surface area. The tMLC is plotted as a dashed line and the xMLC (transformed to w_{drug}/w_{MS}) is represented as red dots with 95% prediction interval for a) CCX, b) CIN, and c) PAR in the five MS grades. (For interpretation of the references to colour in this figure legend, the reader is referred to the web version of this article.)

Table 5
Theoretical pore filling capacity (tPFC) of CCX, CIN, and PAR in the different MS grades.

		SY240	SY350	SY430	SY550	SY730
tPFC (wt%)	CCX	68.4	70.8	68.4	51.9	37.3
	CIN	68.7	66.1	60.4	49.4	34.9
	PAR	65.6	62.9	57.0	45.9	31.8

and tMLC of SY730 is not reflected in a larger xMLC. However, in this case the pore volume rather than the available surface area may be the limiting factor for the loading capacity for this MS grade. In order to evaluate this, the theoretical pore filling capacities (tPFC) for all the systems were calculated from (Hong et al., 2016):

$$\text{tPFC} = \frac{V_{MS}\cdot\rho_{drug}}{1 + V_{MS}\cdot\rho_{drug}}\cdot 100\% \quad (2)$$

where V_{MS} is the pore volume of the MS (cm^3/g) and ρ_{drug} is the amorphous density of the drug (see Tables 1 and 2). The calculated tPFC for all the systems are given in Table 5.

As can be seen, the tPFC for the SY240, SY350, SY430, and SY550 systems are larger than the tMLC as a result of higher pore volumes. The lower tPFC for the PAR systems compared to CXX and CIN is due to lower amorphous density. Furthermore, it is clear that the tPFC for all the SY730 systems are indeed in good agreement with the xMLC. For CCX-SY730, CIN-SY730, and PAR-SY730 the tPFC are 37.3, 34.9, and 31.8 wt%, which is comparable to the xMLC of 35.8, 32.9, and 28.8 wt %, respectively. Hence, this means that the pores of SY730 are completely filled by drug molecules, which indicates that the drug loading capacity for this MS grade is depending on the density of these drugs rather than the surface area. The good correlation between the tPFC and xMLC for the SY730 suggests that the amorphous density of the drugs is a good approximation for the density of the drug molecules inside the MS, which allows for estimation of tPFC for any given pore volume.

To summarize the role interplay between MS textural properties and their effect on drug loading capacity, a simplistic illustration of the xMLC, tMLC, and tPFC as a function of MS pore volume and surface area is shown in Fig. 3. As can be seen, the tMLC increases with increasing surface area whereas tPFC decrease as a result of the smaller pore diameter necessary to achieve the higher surface area. The figure can be divided into four zones defined by the tPFC and tMLC lines,

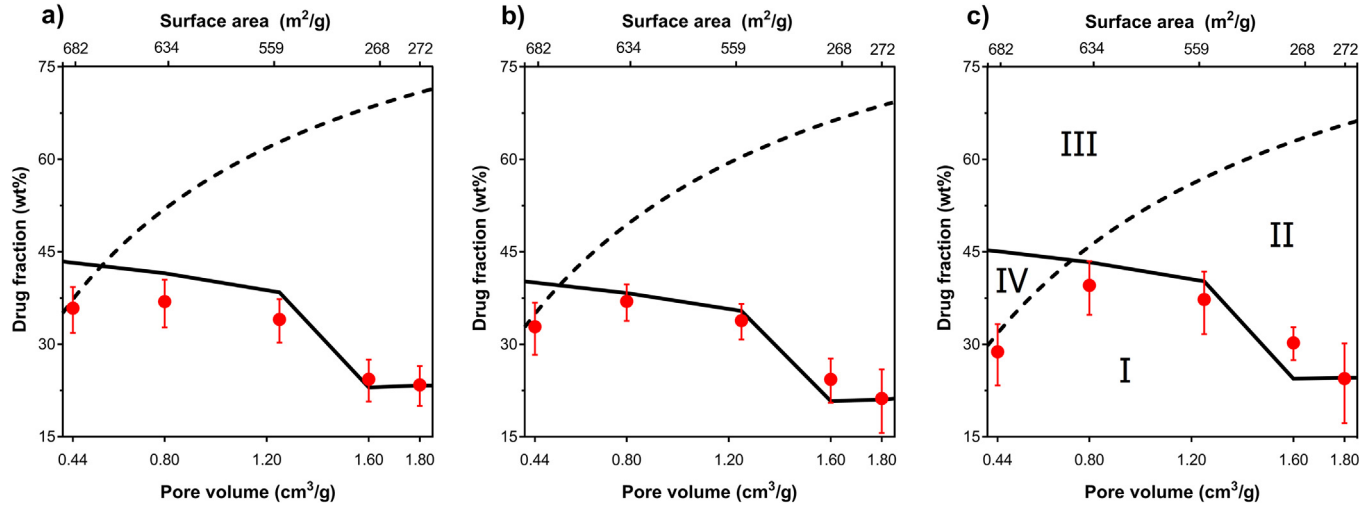

Fig. 3. xMLC (red dots) plotted as a function of MS pore volume and surface area for a) CCX, b) CIN, and c) PAR. The solid lines represents the tMLC and the dashed lines represents the tPFC. In zone I the drug is monomolecularly adsorbed to the MS surface, in zone II the MS pore is filled with drug and in zone III, the pores are overloaded with drug. Zone IV represents a situation where the MS surface is not accessible for the drug molecules and the pores are overloaded with drug. (For interpretation of the references to colour in this figure legend, the reader is referred to the web version of this article.)

which represent four different scenarios. In zone I, the drug fraction is lower than the tMLC and the drug can adsorb monomolecularly to the MS surface. In zone II, the drug fraction is higher than the tMLC and the excess drug will be confined within the pores of the MS. In zone III, the drug fraction is higher than the tPFC and excess drug will be deposited outside the MS pores. The intersection between tMLC and tPFC lines corresponds to a hypothetical situation where the entire surface of MS is covered by monomolecular layer drug and the pores are filled concomitantly. From this point, an increase in surface area (through smaller pore diameter) will not result in an increase of drug loading capacity, but rather a decrease, since the entire surface cannot be monomolecularly covered due to the spatial limitation of the narrow pores. Thus, in zone IV the drug molecules are not able to access the entire available surface area and the drug will be deposited outside the MS pores.

4. Conclusion

In this study, the influence of pore volume and surface area of MS on the MLC was investigated systematically. The findings showed that the xMLC is mainly depending on the minimal projection area of the drug molecule, i.e. the xMLC increase with decreasing drug surface area. In case the MS pores are large enough to accommodate drug-monolayers adsorbed adjacently, a good correlation was obtained between the xMLC and tMLC. However, a decrease in xMLC was observed for the MS grade with the highest surface area, which correlated well with the tPLC rather than the tMLC. This was probably a result of the decreasing pore diameter necessary to accommodate the increasing surface area i.e. if the pore diameter is smaller than the drug molecule, the drug cannot access the available surface area. This means that from a certain point, an increase in MS surface area (through smaller pore diameter) will not result in an increase of drug loading capacity because the entire surface cannot be monomolecularly covered (spatial limitation of the narrow pores). Consequently, for all MS there exists a relationship between surface area and pore volume that will allow for maximum drug loading. With this knowledge, future MS grades may be designed with optimal textural properties for any given drug based on the amorphous density and minimal projection area of the drug molecule.

Declaration of interest

None.

References

Ahern, R.J., Hanrahan, J.P., Tobin, J.M., Ryan, K.B., Crean, A.M., 2013. Comparison of fenofibrate-mesoporous silica drug-loading processes for enhanced drug delivery. Eur. J. Pharm. Sci. 50, 400–409.

Andersson, J., Rosenholm, J., Areva, S., Lindén, M., 2004. Influences of material characteristics on ibuprofen drug loading and release profiles from ordered micro- and mesoporous silica matrices. Chem. Mater. 16, 4160–4167.

Azaïs, T., Tourné-Péteilh, C., Aussenac, F., Baccile, N., Coelho, C., Devoisselle, J.-M., Babonneau, F., 2006. Solid-state NMR study of ibuprofen confined in MCM-41 material. Chem. Mater. 18, 6382–6390.

Charnay, C., Bégu, S., Tourné-Péteilh, C., Nicole, L., Lerner, D.A., Devoisselle, J.M., 2004. Inclusion of ibuprofen in mesoporous templated silica: drug loading and release property. Eur. J. Pharm. Biopharm. 57, 533–540.

Heikkilä, T., Salonen, J., Tuura, J., Hamdy, M.S., Mul, G., Kumar, N., Salmi, T., Murzin, D.Y., Laitinen, L., Kaukonen, A.M., Hirvonen, J., Lehto, V.P., 2007. Mesoporous silica material TUD-1 as a drug delivery system. Int. J. Pharm. 331, 133–138.

Hempel, N.-J., Brede, K., Olesen, N.E., Genina, N., Knopp, M.M., Lobmann, K., 2018. A fast and reliable DSC-based method to determine the monomolecular loading capacity of drugs with good glass-forming ability in mesoporous silica. (Report). Int. J. Pharm. 544, 153.

Hillerström, A., Andersson, M., Samuelsson, J., van Stam, J., 2014. Solvent strategies for loading and release in mesoporous silica. Colloid Interface Sci. Commun. 3, 5–8.

Hong, S., Shen, S., Tan, D.C.T., Ng, W.K., Liu, X., Chia, L.S.O., Irwan, A.W., Tan, R., Nowak, S.A., Marsh, K., Gokhale, R., 2016. High drug load, stable, manufacturable and bioavailable fenofibrate formulations in mesoporous silica: a comparison of spray drying versus solvent impregnation methods. Drug Deliv. 23, 316–327.

Horcajada, P., Rámila, A., Pérez-Pariente, J., Vallet, R.X.M., 2004. Influence of pore size of MCM-41 matrices on drug delivery rate. Microporous Mesoporous Mater. 68, 105–109.

Jackson, M.J., Toth, S.J., Kestur, U.S., Huang, J., Qian, F., Hussain, M.A., Simpson, G.J., Taylor, L.S., 2014. Impact of polymers on the precipitation behavior of highly supersaturated aqueous danazol solutions. Mol. Pharm. 11, 3027–3038.

Kumar, D., Chirravuri, S.S., Shastri, N.R., 2014. Impact of surface area of silica particles on dissolution rate and oral bioavailability of poorly water soluble drugs: a case study with aceclofenac. Int. J. Pharm. 461, 459–468.

Lai, J., Lin, W., Scholes, P., Li, M., 2017. Investigating the effects of loading factors on the in vitro pharmaceutical performance of mesoporous materials as drug carriers for ibuprofen. Materials 10.

Laitinen, R., Löbmann, K., Strachan, C.J., Grohganz, H., Rades, T., 2013. Emerging trends in the stabilization of amorphous drugs. Int. J. Pharm. 453, 65–79.

Limnell, T., Santos, H.A., Mäkilä, E., Heikkilä, T., Salonen, J., Murzin, D.Y., Kumar, N., Laaksonen, T., Peltonen, L., Hirvonen, J., 2011. Drug delivery formulations of ordered and nonordered mesoporous silica: comparison of three drug loading methods. J. Pharm. Sci. 100, 3294–3306.

McCarthy, C.A., Ahern, R.J., Dontireddy, R., Ryan, K.B., Crean, A.M., 2016. Mesoporous silica formulation strategies for drug dissolution enhancement: a review. Expert Opin. Drug Deliv. 13, 93–108.

Mellaerts, R., Mols, R., Jammaer, J.A.G., Aerts, C.A., Annaert, P., Van Humbeeck, J., Van den Mooter, G., Augustijns, P., Martens, J.A., 2008. Increasing the oral bioavailability of the poorly water soluble drug itraconazole with ordered mesoporous silica. Eur. J. Pharm. Biopharm. 69, 223–230.

Qian, K.K., Bogner, R.H., 2011. Spontaneous crystalline-to-amorphous phase transformation of organic or medicinal compounds in the presence of porous media, part 1: thermodynamics of spontaneous amorphization. J. Pharm. Sci. 100, 2801–2815.

Qian, K.K., Bogner, R.H., 2012. Application of mesoporous silicon dioxide and silicate in oral amorphous drug delivery systems. Hoboken 444–463.

Qu, F., Zhu, G., Huang, S., Li, S., Sun, J., Zhang, D., Qiu, S., 2006. Controlled release of Captopril by regulating the pore size and morphology of ordered mesoporous silica. Microporous Mesoporous Mater. 92, 1–9.

Rengarajan, G.T., Enke, D., Steinhart, M., Beiner, M., 2008. Stabilization of the amorphous state of pharmaceuticals in nanopores. J. Mater. Chem. 18, 2537–2539.

Rouquerol, J., Avnir, D., Fairbridge, C.W., Everett, D.H., Haynes, J.M., Pernicone, N., Ramsay, J.D.F., Sing, K.S.W., Unger, K.K., 1994. Recommendations for the characterization of porous solids (Technical Report). Pure Appl. Chem. 66, 1739–1758.

Shen, S.C., Ng, W.K., Chia, L., Dong, Y.C., Tan, R.B., 2010. Stabilized amorphous state of ibuprofen by co-spray drying with mesoporous SBA-15 to enhance dissolution properties. J. Pharm. Sci. 99, 1997–2007.

Yani, Y., Chow, P.S., Tan, R.B.H., 2016. Pore size effect on the stabilization of amorphous drug in a mesoporous material: insights from molecular simulation. Microporous Mesoporous Mater. 221, 117–122.

Zhang, Y., Zhi, Z., Jiang, T., Zhang, J., Wang, Z., Wang, S., 2010. Spherical mesoporous silica nanoparticles for loading and release of the poorly water-soluble drug telmisartan. J. Control. Release 145, 257–263.